Pattern formation and competition in photorefractive oscillators

F. T. Arecchi,[a] S. Boccaletti,[a] G. P. Puccioni, P. L. Ramazza, and S. Residori
Istituto Nazionale di Ottica, 50125 Firenze, Italy

(Received 6 July 1994; accepted for publication 27 July 1994)

We introduce a general model of pattern formation in optical systems made of a cavity with an active medium as a photorefractive crystal fed by a pump. The model is based on the interplay of a diffractive equation for the optical field and a diffusive equation for the medium refractivity. The aim of the model is to describe a series of experiments which have shown mode competition (periodic or chaotic alternation) for low Fresnel numbers (F) and mode coexistence, leading to short range space correlations, for high F. For low F, a linear stability analysis provides the set of modes above threshold as a function of the transverse wave number. Due to the interplay of the optical and the diffusive interactions, different behaviors result depending on the thickness of the medium as compared to the optical absorption length and diffusion length. Including the leading nonlinearities compatible with the symmetry constraints, we introduce normal form equations which describe the time-dependent mode competition. In the case of a large number of modes (high F), nonlinear mode–mode interaction is equivalent to a self-induced noise. In this limit, the relevant feature to be compared with the experiment is the power spectrum.

I. INTRODUCTION

The paradigm of morphogenetic phenomena is the Turing model[1] of two chemical species coupled by reaction diffusion equations, one species being the activator and the other the inhibitor. The concentration fields $c_i(r,t)$ $(i=1,2)$ of the two species can destabilize out of the uniform solution toward time-independent patterns with a length scale of the order of $(l_1 l_2)^{1/2}$ [$l_i=(D_i\tau_i)^{1/2}$ is the diffusion length of species i, having diffusion constant D_i and relaxation time τ_i] provided that $\tau_1\simeq\tau_2$ and $D_1\ll D_2$. For different parameters, the fields can be uniform in space but time dependent (Hopf instability[2]). Finally Turing morphogenetic equations may also provide both space- and time-dependent phenomena (Turing–Hopf patterns).[3]

The main feature of Turing morphogenesis is that the patterns are independent from boundary parameters as well as from the geometry of the containers, since the only sizes which matter are those appearing in the equations of motion.

In the optical case, morphogenesis emerges from the interaction of an optical field ruled by a diffractive equation, with a medium susceptibility ruled by a diffusion equation. Optical morphogenesis, being ruled by diffraction, that is, by coherent transport of a phase term over a given length, provides pattern sizes which depend on some geometric parameter of the cavity.[4] The coupling with the diffusive medium has been so far considered in the thin medium case (longitudinal size of the medium smaller than the diffusion length[5,6]).

A further distinction to be introduced is that between passive and active optical morphogenesis. In the former case, an input field is distorted while propagating in a closed loop (cavity containing an optical medium). In the latter one, the intracavity medium is fed by an external pump and the corresponding excitation gives rise to the spontaneous emergence of a cavity field. Thus, passive morphogenesis consists in the distortion of a uniform input field toward a new configuration, while active morphogenesis consists in the appearance of a field out of vacuum. The most studied passive system is a cavity with a Kerr medium within which a field undergoes a dephasing, and which has a source term proportional to the square of the field.[5,6] This case has been dealt with in many experimental situations, including nonlocal interaction due to rotation and translation of the transverse optical pattern in the feedback loop.[7–10]

For the active case, one class widely studied is that of laser phenomena, where the active medium is usually modeled as a collection of pumped two level atoms.[11–13] Another class, on which there is a wealth of experimental studies, is that of the photorefractive oscillators.[14–22] The main advantage of the photorefractive optics is that its time scales are so slow, that many transient features can be followed in real time and compared with the model, whereas in the laser case only time-integrated patterns are available thus far, and a breakthrough is necessary in order to reach a satisfactory match between models and experiments. This paper is an attempt to build a coherent model for photorefractive morphogenesis, comparing the theoretical results with the wealth of experimental features reported recently.

In these systems the active medium is an array of dipoles made of free electrons and fixed donors. In the dark, the donor atoms are neutrals. As a pump and a signal field impinge on the medium, the large intensity corresponding to the interference peaks ionize the donors yielding a space charge field of free electrons. The space charge undergoes local relaxation (recombination processes), diffusion, and drift in the presence of an applied DC field. The space charge grating scatters energy from the pump into the signal direction. Even in the absence of a macroscopic signal field (signal in the vacuum state), the creation operator of the signal field starts the process. As in the case of the lasers, even though the initial seed is quantum, a classical description is sufficient for all purposes.

The geometry of the experiment is shown in Fig. 1. For a fixed pump intensity and angle θ between pump and cavity

[a]Also at Department of Physics, University of Firenze, Firenze, Italy.

 1054-1500/94/4(3)/491/8/$6.00

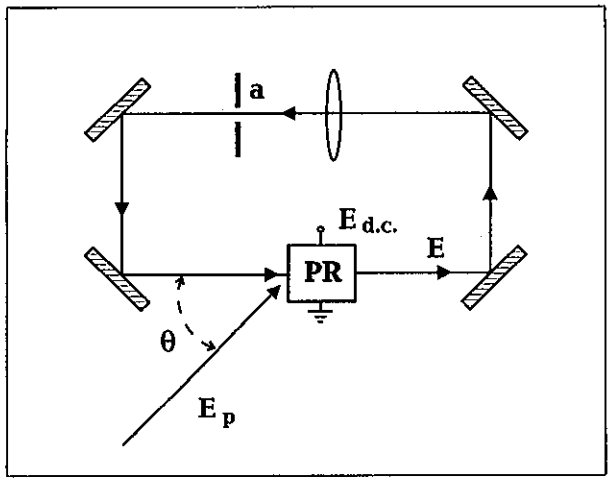

FIG. 1. Schematic setup of active optical morphogenesis. The photorefractive crystal (PR), of thickness l, is pumped by a laser field E_p and driven by a transverse DC voltage E_{DC}. The emitted field is confined in a ring cavity made of four mirrors, a lens, and a pupil a which controls the Fresnel number. The free propagation length d in which diffraction is effective is the fraction of the overall cavity length L not compensated by the imaging properties of the lens.

axis, the dynamics is ruled by two control parameters, the DC field E_{DC} applied across the crystal, in a direction parallel to the grating wave vector, and the aperture a of the pupil of the cavity, which controls the Fresnel number F, that is, the number $N=F^2$ of cavity modes. Here we call cavity modes the free field configurations allowed by the boundary conditions; E_{DC} imposes a drift velocity to free charges, and hence a Doppler shift between incident and scattered wave.

Increase of the extensive parameter F for fixed pump and E_{DC} induces a series of bifurcations described in Ref. 16. For low $F(F\leqslant 4)$ a single mode per time appears, but a given number N of modes, limited by the relation $N\leqslant F^2$, competes sequentially. This means that each of the N modes survives for a given time, and then it is replaced by another one and so on, in a periodic fashion. This phenomenon was called periodic alternation (PA). It differs from the so-called antiphase states[23] insofar as only one specific ordered sequence appears, that in which the mode azimuthal number decreases from the largest value to zero, and then it jumps again to the largest one, and so on. This sequence is regularized when an axial stop quenches the TEM_{00} (on axis) mode.[15] As a matter of fact, an annular diaphragm provides a sequence of competing modes as shown in Fig. 3 of Ref. 15, where the modes differ only for the azimuthal quantum number. For increasing $F(F\sim 4)$ the persistence time of each mode is irregular (chaotic alternation: CA). Away from the narrow switching time intervals, both in PA and CA the amount of mode mixing is negligible.

A phenomenon similar to CA, called chaotic itinerancy, was introduced by Ikeda *et al.*,[24] Otsuka,[25] Kaneko,[26] and Tsuda[27] in dealing with numerical solutions of different classes of model equations, namely, a one-dimensional laser,[24] an array of coupled lasers,[25] globally coupled iteration maps,[26] and nonequilibrium neural networks.[27] In fact, this latter phenomenon includes erratic jumps among the available quasistationary states, whereas CA keeps the sequence ordering. Such is the case in the experiment of Ref. 15, even though it was initially called chaotic itinerancy.

Both in PA and CA the existence of one mode per time is confirmed by measuring the spatial correlation function $C(\rho)$ of the intensity fluctuations $\delta I(r,t)=I(r,t)-\langle I(r,t)\rangle$, where $\langle\ \rangle$ denotes time average,[28]

$$C(\rho)=\langle \delta I(0,t)\,\delta I(\rho,t)\rangle, \tag{1}$$

and checking that $C(\rho)$ has a decay length equal to the wavefront size.

As F increases, pure cavity modes no longer alternate but they coexist at the same time with little mutual correlation, as shown by the shrinking of the correlation length. The many bright spots which are observed on the wave front or, equivalently, the intermingled dark spots giving rise to phase singularities, are no longer lying in a regular pattern. In fact what we now observe is an almost stochastic pattern. In analogy with the hydrodynamic models[28] this regime is called space–time chaos (STC) and it may be characterized in terms of the statistical moments of the local fluctuations as done in Ref. 15.

The phenomenology summarized here appears unusual as compared with previous treatments of space–time instabilities of extended nonlinear excited media.

Two different models are currently used to describe light-induced charge transport in photorefractive materials: the band transport model by Kukhtarev *et al.*[29] and the hopping model by Feinberg *et al.*[30] In the Feinberg model, charge carriers are assumed to experience jumps among trap sites, with a rate which is function of the distance. The Kukhtarev band transport model involves coherent motion of the photoexcited carriers between scattering events by lattice imperfections and phonons. In fact, both models provide essentially equivalent descriptions of the process,[31] although they use a different language and a different set of physical parameters. However, the band transport model is more generally used and is better accommodated in the standard analysis of carrier migration in insulating and semiconductor materials. For these reasons, we will also make use of this model.

The paper is organized as follows. In Sec. II we derive the coupled field and material equations. As for the latter one, we introduce an equivalent collective dynamics, based on the relevant measured space and time scales, and accounting also for saturation.

In Sec. III we perform a linear stability analysis and classify the band of unstable modes and we consider a set of fixed point solutions coupled by the leading nonlinearities compatible with the symmetry constraints (normal form equations) and thus we recover the observed phenomena of mode competition (PA and CA). In Sec. IV we consider the high Fresnel number regime. In such a case, all modes below threshold provide a self-induced noise input. We will show that this is the equivalent in wave-number space of the noise induced by the modes below threshold in frequency space in the one-dimensional laser model (Maxwell–Bloch turbulence[24]). The presence of a noise source forbids a de-

terministic treatment. It provides an explanation for the short range space correlations which characterize the high F regime. Taking the noise as white, we can evaluate the power spectrum of the emitted field and compare it with the experiment.

II. MODEL EQUATIONS

We aim at building a specific model which contains all the relevant physical aspects of the experiment described above without recurring to unnecessary microscopic assumptions. The requirement is that all the relevant parameters should be characterized by the experimental setup shown in Fig. 1 plus the addition of simple optical measurement of bulk properties done on the crystal without cavity.[20]

The two wave mixing gives rise to a grating which breaks the cylindrical symmetry of the cavity. The grating spacing is

$$\Lambda=\frac{2\pi}{K}=\frac{2\pi}{k_0\theta}, \tag{2}$$

k_0 being the wave number of the pump, and $\theta\ll 1$ the angle between the two waves, which in the experiment[15] is optimized at $\theta\simeq 1/60$ rad.

Introducing an x,y,z coordinate system with z along the cavity axis, x-z being the plane which contains the propagation directions of the two fields E_p and E, and with the origin at the intersection of the input face of the crystal with the cavity axis, the equation for the total field $\tilde{E}=E_p+E$ is

$$\Box^2\tilde{E}=-\mu\partial_t^2 P\ \mathrm{rect}(z/l), \tag{3}$$

where $\mathrm{rect}(z/l)\equiv 1$ for $0<z<l$ and $\mathrm{rect}(z/l)\equiv 0$ elsewhere, l being the crystal thickness. The derivative signs are abbreviated as, e.g., ∂_t^2 for $\partial^2/\partial t^2$, etc.

Since the cavity length L is much longer than l, the source term on the right-hand side is strongly localized. The polarization is given by

$$P=\epsilon_0\chi\tilde{E}, \tag{4}$$

where the susceptibility field $\chi(\mathbf{r}_\perp,z,t)[\mathbf{r}_\perp=(x,y)$ stays for the transverse coordinate] obeys the equation

$$\left(\partial_t+\frac{1}{\tau}-D\nabla^2\right)\chi=f(\tilde{E}), \tag{5}$$

where $\nabla\equiv\partial_x^2+\partial_y^2+\partial_z^2\equiv\nabla_\perp^2+\partial_z^2$.

Equation (5) arises from the following considerations. The two-wave mixing gives rise to a space charge field $\chi(r,t)$, consisting of a dipole distribution created by the offset of the free electrons with respect to the fixed donors in the BSO material. The collective wave χ decays locally with a lifetime τ and diffuses at a rate D. Direct measurement on the crystal used provide a value $\tau\simeq 1$ s (Ref. 20), while values of D reported in the literature[32] are spread in the range 10^{-6}–10^{-10} m^2/s.

In order to solve Eqs. (3)–(5), we first isolate a fast varying part in z and t from the slow space–time dependence which is relevant for the dynamics, by writing

$$\tilde{E}=E_p e^{-i(\mathbf{k}_0\cdot\mathbf{r}-\omega_0 t)}+E(\mathbf{r}_\perp;z,t)e^{-i(kz-\omega t)}. \tag{6}$$

This way, we have extracted from the cavity field a plane wave along the cavity axis (k along z), thus E includes the full dependence on $\mathbf{r}_\perp$ plus the residual slow dependence on z and t.

The applied DC field E_{DC} in the x direction induces a space charge drift, with a speed v_d, thus, from Eq. (2), the scattering grating provides a frequency offset along x given by

$$\Omega=v_d k_0\theta. \tag{7}$$

Consequently, the cavity field has a frequency ω detuned with respect to the pump frequency ω_0, by

$$\omega=\omega_0-\Omega. \tag{8}$$

In the rest of the paper, we will neglect this detuning for the following reasons. As we shall see, calling q the wave number of transverse fluctuations ($|q_{\max}|\simeq 100$ cm^{-1}) diffraction along the free propagation length d inside the cavity introduces a space dephasing $\delta\varphi_1\simeq q^2 d/2k_0\simeq O(1)$ for each q component. On the other hand, since the bandwidth of the active medium is very narrow ($\Delta\nu\simeq 1/\tau\simeq 1$ s^{-1}) and all oscillatory modes are pulled within that line, this means that the mutual dephasing after a round-trip due to different mode frequencies is of the order of $\delta\varphi_2\simeq\Delta\nu L/c\simeq 10^{-8}$, and thus completely negligible with respect to $\delta\varphi_1$. In the following, we will not consider the effects of detuning in the stability analysis.

By use of Eq. (6) and neglecting the second "slow" derivatives (so called eikonal approximation), the $\Box^2$ kernel reduces to $\partial_t+c\partial_z-(ic/2k)\nabla_\perp^2$. Furthermore, we approximate $\partial_t^2 P\approx-\omega^2 P$. By Fourier expansion of the transverse dependence $\mathbf{r}_\perp\to\mathbf{k}$, the product $\chi\tilde{E}$ of Eq. (4) transforms into a convolution. In this one, only the two components

$$\chi_0\equiv\chi(\mathbf{k}=0)$$

and

$$\chi\equiv\chi(-\mathbf{K}=\mathbf{k}-\mathbf{k}_0),$$

multiplied, respectively, by the cavity and pump fields, yield phase matched contributions to Eq. (4). Precisely, Eq. (3) becomes

$$\left(\partial_t+c\partial_z-\frac{ic}{2k}\nabla_\perp^2\right)E=-\frac{i\omega}{2}(\chi_0 E+\chi E_p)\mathrm{rect}\left(\frac{z}{l}\right)$$
$$=\left(-\frac{i\omega}{2}\chi E_p-\Gamma E\right)\mathrm{rect}\left(\frac{z}{l}\right). \tag{9}$$

In writing the last line we have taken into account only the imaginary part of $\chi_0=\chi_0'+i\chi_0''$ through $\Gamma=-(\omega/2)\chi_0''$. This corresponds to a transmission loss of the crystal in the absence of pump which persists unmodified even with pump. The real part of χ_0 induces a renormalization of c which is irrelevant for the field equation, since it has to be weighted by the cavity filling factor $l/L\ll 1$. Thus the material equation (5) provides the evolution for the envelope of the susceptibility

$$\chi=\tilde{\chi}(\mathbf{r}_\perp,z,t)e^{i(Kx-\Omega t)}. \tag{10}$$

By the same argument of separation of fast and slow variables in the longitudinal dependence used in going from Eq. (3) to (9), matching of the phases which appear in the exponentials of (10) and (6) accounts for the "fast" space variations on a scale

$$\frac{2\pi}{K}\equiv\Lambda\simeq\frac{\lambda}{\theta}\simeq 30\ \ \mu\text{m}$$

($\theta\sim 1/60$, $\lambda\sim 0.5\ \mu$m).

By the above scale consideration, we can rewrite the equation for the $\tilde{\chi}$ amplitude as

$$\left(\partial_t+\frac{1}{\tau}-D\nabla^2\right)\tilde{\chi}(r_\perp,z,t)=r\,\frac{E_p^* E}{|E_p|^2}\left(1-\frac{|E|^2}{|E_p|^2}\right), \quad (11)$$

where the source term is derived from the Kukhtarev model, with the assumption $|E|\ll|E_p|$ and r is the complex photorefractive coefficient. It has to be underlined that, in order to derive a single equation starting from the Kukhtarev set of three coupled nonlinear partial differential equations, a projection onto a single plane wave has been adopted.[29] A more complete approach, taking into account also the slow spatial variations of the variables, is still lacking. In order to overcome this difficulty, we relax the single plane wave approximation by introducing a diffusion term in the LHS of Eq. (11). The presence of this diffusion term in the material equation represents an important difference with respect to a recent model for a photorefractive oscillator.[33] Furthermore, that model is specialized to the case $E_{DC}=0$, thus leading to a purely imaginary r coefficient. The left-hand side of Eq. (11) is justified as follows: $\tilde{\chi}$ is due to the dipole array made by free electrons and fixed donors. It is quenched either by local recombination processes (relaxation time τ) or by diffusion of electrons.

The wave number K at which the Bragg scattering line has to be positioned was measured by optimizing the photorefractive gain in a single pass amplification.[20]

The coupled equations (9) and (11) describe the dynamics of the photorefractive oscillator. The two equations imply two very different time scales. Integration of Eq. (9) over z includes the right-hand source term on a thin slice $l\ll L$ plus a free propagation along the rest of the cavity of length $L-l\sim L$. Since $L\simeq 2$ m the transit time on the ring takes a few nanoseconds. Furthermore, since the intracavity losses for forward propagation are very high (BSO has a transmission 15%), the overall cavity damping time t_c is shorter than 100 ns. On the contrary, the material excitation χ decays over a time scale $\tau\sim 1$ s.

III. THE LOW *F* LIMIT

A. Linear stability analysis

If the Fresnel number is small, only a few modes propagating close to the cavity axis will be allowed, since the finite mirror size introduces losses rapidly increasing with the transverse wave number q. We will show that a stability analysis of the coupled field and medium equations (9) and (11), around the stationary solution corresponding to zero field $E=0$ and thus zero susceptibility $\tilde{\chi}=0$, will provide oscillatory q bands within which modes are oscillating. Then (Sec. III B) we will include the leading nonlinearities which induce a mode–mode competition. Let us introduce an optical field normalized to the pump field,

$$y=E/E_p$$

and for simplicity denote by χ the amplitude $\tilde{\chi}$ around wave number K.

The linearized coupled equations are

$$\left(\partial_t+c\partial_z-i\,\frac{c}{2k}\,\nabla_\perp^2\right)y=\left(-i\,\frac{\omega}{2}\,\chi-\Gamma y\right)\text{rect}\left(\frac{z}{l}\right), \quad (12)$$

$$(\partial_t+1-l_D^2\nabla^2)\chi=ry. \quad (13)$$

In writing Eq. (13), we introduce $l_D^2=D\tau$ and normalize the time scale to τ. Since experimental evidence has provided $\tau\sim 1$ s, this normalization is not formally affecting Eq. (12). Since the time evolution of the field is much faster than that of the material variables, the field equation within the medium reduces to

$$\left(\partial_z-\frac{i}{2k}\,\nabla_\perp^2\right)y=i\,\frac{k}{2}\,\chi-\gamma y \quad (14)$$

where $\gamma=\Gamma/c$.

Our treatment differs from all previous ones for two innovative elements, namely,

(i) in Eq. (13) we do not limit to a diffusively thin slice of length $l\ll l_D$, but account also for longitudinal diffusion;

(ii) in Eq. (14) we keep the diffraction term even within the medium. In previous treatments,[5,6,33] this term was canceled, in view of a short propagation length l within the medium as compared to the cavity length L. In our case, due to the insertion of the intracavity lens (Fig. 1), most of the propagation is constrained by an optical imaging (object to image plane) for which diffraction is compensated.[34] Thus the free propagation length d may be much less than the overall cavity length, so that $l/d\sim O(1)$.

We Fourier transform in the transverse coordinate $\mathbf{r}_\perp\to\mathbf{q}$, keeping for the time being the longitudinal z dependence. Thus Eq. (14) becomes [to simplify the notation, we do not use different symbols for $y(\mathbf{r}_\perp,z,t)$ and $y(\mathbf{q},z,t)$, since the meaning emerges from the context]

$$\partial_z y=\alpha\chi-\gamma_q y, \quad (15)$$

where $\gamma_q=\gamma+i(q^2/2k)$ and $\alpha=(ik/2)$. We conceptually split the medium slab into a large number n of longitudinal slices of length $\Delta=l/n$ such that $\chi(z)$ is uniform over Δ, and then let $\Delta\to 0$.

Calling y_j the output field from the jth slab, χ_j the susceptibility taken as uniform over Δ and y_{j-1} the input field, integration of (15) over the jth slab yields

$$y_j=y_{j-1}e^{-\gamma_q\Delta}+\frac{\alpha}{\gamma_q}\,\chi_j(1-e^{-\gamma_q\Delta}). \quad (16)$$

We now Fourier transform for the longitudinal dependence $j\to h$. In the $\mathbf{q}$-h space, the above equation can be written as

$$y_h = y_h e^{-ih\Delta} e^{-\gamma_q \Delta} + \frac{\alpha}{\gamma_q} \chi_h (1 - e^{-\gamma_q \Delta}), \tag{17}$$

where we shorthand y_h for $y(\mathbf{q},h,t)$ and have used the translation formula

$$y_{j-1} \rightarrow y_h e^{-ih\Delta}. \tag{18}$$

In the same $\mathbf{q}$-h space, the medium equation is written as

$$[\partial_t + 1 + l_D^2(q^2 + h^2)]\chi_h = r y_h e^{-ih\Delta}, \tag{19}$$

since the source term for χ_j is y_{j-1}.

If we now consider an exponential time dependence as

$$\chi(\mathbf{q},h,t) = \chi_h e^{\lambda t}$$

so that $\partial_t \rightarrow \lambda$, then Eq. (19) yields the formal solution

$$\chi_h = r D_{qh}^{-1} y_h e^{-ih\Delta}, \tag{20}$$

where

$$D_{qh} \equiv \lambda + 1 + l_D^2(q^2 + h^2). \tag{21}$$

Placing Eq. (20) into (17) we have

$$y_h = y_h e^{-ih\Delta}\left(e^{-\gamma_q \Delta} + \frac{\alpha}{\gamma_q} r D_{qh}^{-1}(1 - e^{-\gamma_q \Delta}) \right). \tag{22}$$

On the other hand, the stationary free space (source free) solution of Eq. (12) over a propagation length d yields in real longitudinal space j

$$y_0 = y_n e^{-iq^2 d/2k}. \tag{23}$$

In h space, in view of the longitudinal translation factor e^{-ihl}, Eq. (23) permits one to express h as a function of q as

$$h = \frac{q^2 d}{2kl}. \tag{24}$$

Solving Eq. (22) for the kernel D_{qh} one finds

$$D_{qh} = \frac{\alpha}{\gamma_q} r \frac{1 - e^{-\gamma_q \Delta}}{e^{ih\Delta} - e^{-\gamma_q \Delta}}.$$

It is very easy to evaluate the $\Delta \rightarrow 0$ limit of the above expression, which is

$$D_{qh} = \alpha r \frac{1}{ih + \gamma_q}, \tag{25}$$

which, by use of (21) and (24), yields the dependence of the eigenvalues λ upon the transverse wave number q

$$\lambda = -1 - l_D^2\left(q^2 + \frac{d}{2kl} q^4 \right) + \alpha r \frac{1}{(i/2k)(1 + d/l)q^2 + \gamma}. \tag{26}$$

The real part of λ is plotted in Fig. 2, together with the wave-number position of the lowest order transverse models TEM_{00} and $TEM_{01/10}$. We see that the first one is below threshold while the other two are above, for realistic parameter values as shown in the caption of Fig. 5. In the linear limit only the modes above threshold are excited. However, introduction of the leading nonlinearities compatible with the symmetry constraints may give rise to a competing dynamics with the probability of temporarily quenching of modes on behalf of modes linearly below threshold as described in the next subsection.

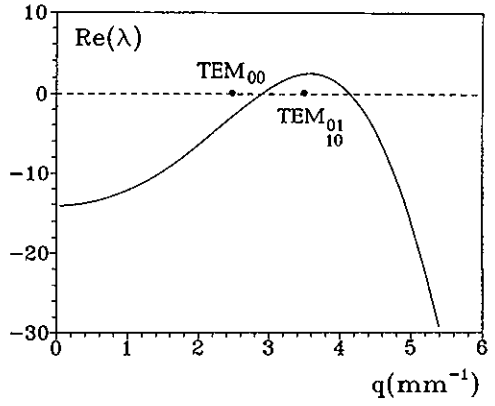

FIG. 2. Linear stability diagram. The real part of λ is plotted versus the transverse wave number $q(\mathrm{mm}^{-1})$. Only the modes with $\Re\lambda > 0$ can be linearly excited. We show the q position of the lowest transverse modes which are put in interaction by the nonlinearities. $\mu = -25$, $\nu = 400$, $l_D = 330$ μm, $d = 2.5$ cm, $l = 1$ cm, $\gamma = 1.9$ cm^{-1}.

B. Normal form equations

For low Fresnel number, only a few modes of the cavity are allowed to oscillate in the resonator. Hence, it is possible to project Eqs. (9) and (11) onto these modes, thus obtaining a set of ordinary differential equations. In this boundary-dependent regime it is possible to account for the basic phenomena observed on the simple basis of symmetry arguments.[11,19] Use of symmetry arguments provides directly the simplest nonlinear interaction (normal form approach[35]). Such an argument is applied to the photorefractive oscillator in Ref. 19 and here below we review that approach.

For the sake of simplicity, let us consider a simple dynamics involving three transverse modes, a central one with amplitude z_0 and two higher order ones counter-rotating along the azimuthal coordinate φ with respective amplitudes z_1 and z_2 and angular momenta ± 1. We can expand the cavity field as

$$E = f_1(r,l)(z_1 e^{i\varphi} + z_2 e^{-i\varphi}) e^{i\omega_1 t} + f_0(r,l) z_0 e^{i\omega_0 t},$$

where f_0 and f_1 are the space distributions of the modes. The optical frequencies ω_0 and ω_1 are in general different, and slow time dependence due to the dynamics is included in the amplitudes $z_i(t)$ $(i = 0,1,2)$.

The zero intensity situation corresponds to $z_0 = z_1 = z_2 = 0$, the central mode to $z_1 = z_2 = 0$ and an azimuthal standing wave to $z_0 = 0$, $z_1 = z_2$.

The time sequence of these three situations is one of the simplest cases experimentally observed,[15] so we aim at building model equations having the above sets of z values as fixed points. Since, however, any quasistationary point persists for a finite time, each of the fixed points must have at least an unstable direction. With these general rules in mind we now discuss the symmetry requirements.

The observed symmetries impose the following constraints on the mode amplitudes:[35]

$$\Theta:(z_1,z_2,z_0)\rightarrow(e^{i\varphi}z_1,e^{-i\varphi}z_2,z_0), \tag{27}$$

$$K:(z_1,z_2,z_0)\rightarrow(z_2,z_1,z_0), \tag{28}$$

where Θ denotes the rotation operation, and K the reflection around the privileged plane. As these modes are born by Hopf bifurcations, there is an additional time symmetry

$$B:(z_1,z_2,z_0)\rightarrow(e^{i\beta_1}z_1,e^{i\beta_1}z_2,e^{i\beta_0}z_0). \tag{29}$$

The normal form for the nonlinear interaction among the three modes, assuming that the symmetry of the system is Z_2 (reflection) degenerated toward an $O(2)$ one (reflection and rotation) is[11,36] (dots denote time derivatives)

$$\begin{aligned}\dot{z}_0&=\lambda_0 z_0+[a(|z_1|^2+|z_2|^2)+b|z_0|^2]z_0,\\ \dot{z}_1&=\lambda_1 z_1+(c|z_1|^2+d|z_2|^2+e|z_0|^2)z_1+\epsilon z_2,\\ \dot{z}_2&=\lambda_1 z_1+(d|z_1|^2+c|z_2|^2+e|z_0|^2)z_2+\epsilon z_1,\end{aligned} \tag{30}$$

where $\lambda_0,\lambda_1,a,b,c,d,e$ are complex coefficients and $\epsilon=\rho_\epsilon e^{i\varphi_\epsilon}$ is a symmetry breaking parameter, accounting for the breakup of the cylindrical symmetry due to the experimental setup which introduces a privileged plane (that containing the directions of both pump and signal beam).

Letting $z_i = \rho_i e^{i\varphi_i}$, and changing the variables as $\rho_1=A\cos(\alpha/2)$, $\rho_2=A\sin(\alpha/2)$ and $\alpha=\varphi_2-\varphi_1$, it is found that in the (ρ_0,A) plane of the phase space there are three fixed points O, SW, and C, corresponding, respectively, to the off state of the oscillator, TEM_{10} (or TEM_{01}) mode and TEM_{00} mode.

It is possible to show that, for certain values of the parameters λ_i,a,b,c,d,e (see Ref. 19 for details), a fourth fixed point exists in the (ρ_0,A) plane. The Hopf bifurcation of this fixed point can result in limit cycles that forms heteroclinic connections among points O, SW, and C. In particular, for obtaining the observed PA and CA phenomena it is necessary to have a subcritical bifurcation for one of the modes. This imposes that one of the linear coefficients λ_i of Eq. (30) be negative. This is in fact what happens in our system, as shown in Sec. III A.

The corresponding phase portrait in the (ρ_0,ρ_1) plane (we recall that $|\rho_1|=|A|$) is shown in Fig. 3. As a periodic orbit emerging from P gets close to the other fixed points, there will be a critical slowing down that will give rise to the periodic alternation phenomenon among the O, SW, and C states.

The phenomenology of chaotic alternation can be understood on the basis of the normal form approach also. Indeed, in the experiment of Ref. 15 a strong pulling action due to the narrow frequency width of the photorefractive medium provides equal dressed frequencies for all transverse modes, even though the bare frequencies were different. Now, Eqs. (30) refer to the modes dressed by their interaction with the medium, hence a frequency degeneracy $\omega_1=\omega_0$ should be included. A resonance between the states with angular momenta ±1 and the central one implies an additional symmetry. Namely the time symmetry becomes[35]

$$B:(z_1,z_2,z_0)\rightarrow(e^{i\beta}z_1,e^{i\beta}z_2,e^{i\beta}z_0). \tag{31}$$

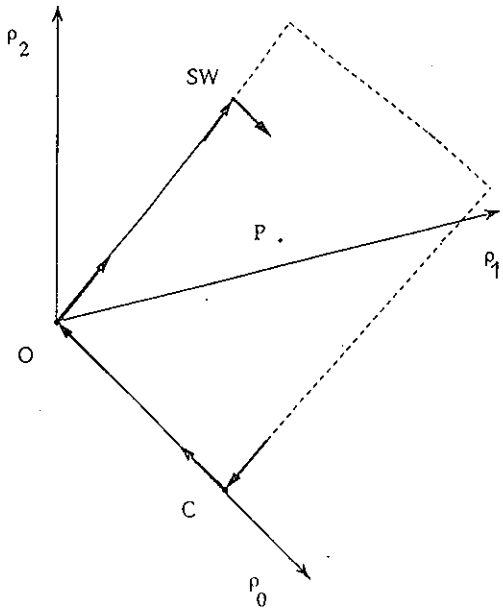

FIG. 3. Three-dimensional (ρ_0,ρ_1,ρ_2) projection of the phase space. The arrows indicate the local stability properties of the zero (0), central (C) and standing wave (SW) solutions, which lie on the (ρ_0,A) plane (sketched by dashed lines).

This allows additional terms to survive in the normal form equation, which will now read as follows:

$$\begin{aligned}\dot{z}_0&=\lambda_0 z_0+[a(|z_1|^2+|z_2|^2)+b|z_0|^2]z_0+fz_1z_2z_0^*,\\ \dot{z}_1&=\lambda_1 z_1+(c|z_1|^2+d|z_2|^2+e|z_0|^2)z_1+\epsilon z_2+gz_0^2z_2^*,\\ \dot{z}_2&=\lambda_1 z_1+(d|z_1|^2+c|z_2|^2+e|z_0|^2)z_2+\epsilon z_1+gz_0^2z_1^*,\end{aligned} \tag{32}$$

where f and g are complex coefficients. Dynamically, the additional terms due to resonance act as forcing terms with frequency $2\dot{\varphi}_0-(\dot{\varphi}_1+\dot{\varphi}_2)$, thus inducing dramatic changes in the structure of the solutions.

Notice that if the additional terms are "turned on" when the other parameters are tuned close to an heteroclinic solution, some of the periodic solutions can disappear, some can bifurcate to solutions of different periodicity, and even chaotic behavior can be expected. Figure 4 reports the phase portrait arising from Eqs. (32). Notice the existence of a chaotic solution getting close to the pure modes (CA). Both PA and CA phenomena are structurally stable, insofar as they persist over wide ranges of parameter values.

IV. THE HIGH FRESNEL NUMBER LIMIT

The solution for the field and matter linearized equations, discussed in the previous section, remains valid even in the case of high Fresnel number. However, since in this last case a large number of modes are simultaneously allowed to be above threshold, we have a high dimensional dynamical system characterized by a space–time chaotic behavior, for which a description in terms of modal amplitude time evolution becomes of poor significance.

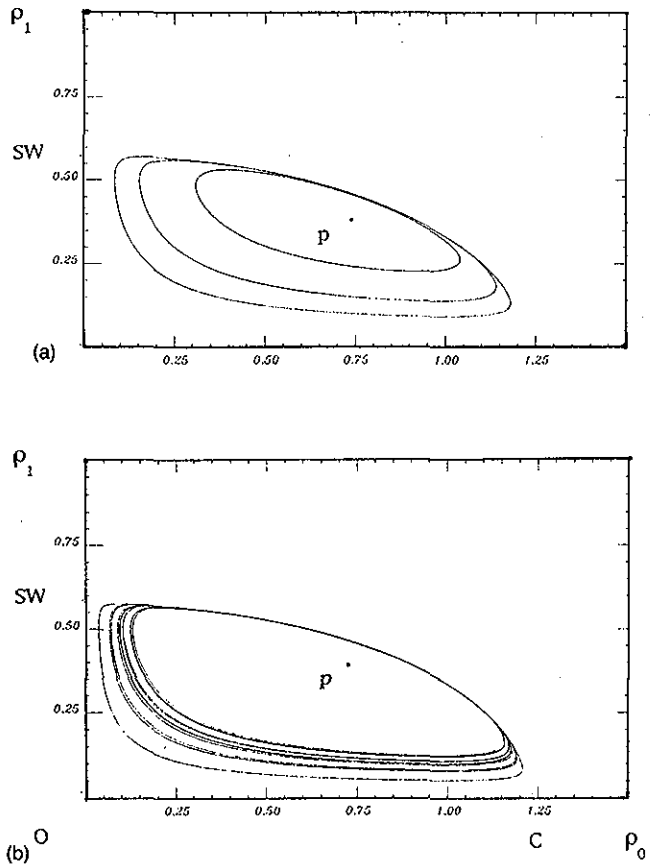

FIG. 4. (a) (ρ_0,ρ_1) projection of the solutions of Eqs. (30) for $a^r=3$, $b^r=1$, $c^r=-1$, $d^r=-2$, $e^r=-1$, $\lambda_1^r=0.5$, $\lambda_0^r=-1.5$, $\rho_\epsilon=0.5$, $\varphi_\epsilon=0$, $c^i=d^i=1$. P is marginally stable and for any initial condition a periodic orbit is found. The closer a period orbit is to the three fixed points, the larger the period. The imaginary parts of the coefficients $\lambda_{0,1}$, b, a and e contribute only to the dynamical evolution of φ_0 and φ_1; (b) (ρ_0,ρ_1) projection of a chaotic solution of Eqs. (32). Same parameter values as in (a) plus $f^r=-0.01$, $g^r=0.02$, $f^i=0$, $g^i=0$.

The space–time chaotic state has been experimentally characterized in terms of a correlation length much shorter than the whole extension of the transverse signal,[15] and of an exponentially decaying power spectrum with a spatial frequency cutoff $q_c\simeq 200\ \mu$m.[20] This means that, in this regime, the optical field behaves like a set of uncorrelated domains of a size much smaller than the transverse wave front. According to this experimental evidence, we can still consider the linear evolution of each spectral susceptibility component as ruled by a separate equation, however affected by a "fictitious" noise source.

Precisely, we introduce a projection operator P and its conjugate $Q=1-P$ over the whole space of spectral modes. By P we pick up those modes of which we intend to describe the dynamics, and by Q we collect all the other modes which act as noise. The nonlinearities couple the two subspaces spanned by P and Q, so that the P subspace still obeys equations as reported in Sec. III, while the Q subspace acts as a noise source on the previous one.

We account for the experimental fact that, for high F, the correlation length is much smaller than the transverse domain size, by introducing a Gaussian noise source N with zero average and δ correlated in space and time (white noise in frequency and wave number) that is

$$\langle N\rangle=0,$$
$$\langle N^*(z,\mathbf{r}_\perp,t)N(z',\mathbf{r}'_\perp,t')\rangle=\sigma\delta(t-t')\,\delta(z-z')\,\delta(\mathbf{r}_\perp-r'_\perp). \tag{33}$$

In the spectral domain, we have seen [Eq. (19)] that

$$D_{qh}(\omega)\chi_h=ry_he^{-ih\Delta}, \tag{34}$$

where $D_{qh}(\omega)=i\omega+1+l_D^2(q^2+h^2)$.

Besides the source due to the (h,q) field mode as given by the right-hand side (P space projection), we must add a noise contribution (global contribution of the Q space), so that the high F equation becomes

$$D_{qh}(\omega)\chi_h=ry_he^{-ih\Delta}+N. \tag{35}$$

Notice that Eqs. (20) and (25) allow one to express y_h in terms of χ_h in the $\Delta\to 0$ limit as

$$y_h=\frac{\alpha e^{ih\Delta}}{ih+\gamma_q}\chi_h. \tag{36}$$

Replacing (36) into (35), we can solve χ_h in terms of N. Taking the modulus square and averaging over the N distribution by use of (33), we have

$$\langle|\chi_h|^2\rangle=\frac{\sigma}{|i\omega+1+l_D^2(q^2+h^2)-[\alpha r/(ih+\gamma_q)]|^2}. \tag{37}$$

For $\omega=0$, this expression yields the time-averaged power spectrum S_χ of χ_h. The corresponding power spectrum of the optical field is

$$S_y=\frac{|\alpha|^2}{|ih+\gamma_q|^2}S_\chi. \tag{38}$$

Utilizing the relation (24) between h and q, S_y can be expressed as a function of q. An example of this power spectrum for a selected parameter $\alpha r=\mu+i\nu$ is shown in Fig. 5(a) together with the experimental power spectrum [Fig. 5(b)]. The best agreement between experiment and theory is reached for $\mu=-25$ and $\nu=400$.

It is important to note that the power spectrum has nonzero components even at $q\simeq 0$, where the linear stability analysis of Sec. III predicts that the modes are damped. This behavior is reminiscent of the mechanism first introduced in the study of longitudinal multimode lasers, named "Maxwell–Bloch turbulence,"[24] and consisting in a noise-like contribution to the dynamics of modes that are linearly stable via a nonlinear exchange of energy with the linearly unstable modes (self-induced noise).

V. CONCLUSIONS

We have shown that optical morphogenesis arises from the competition between the diffractive properties of the electromagnetic field and the diffusive properties of the medium refractivity. In the low F limit, the diffractive nature of the optical field dominates, and the competition generates boundary dominated instabilities. In the high F limit, each

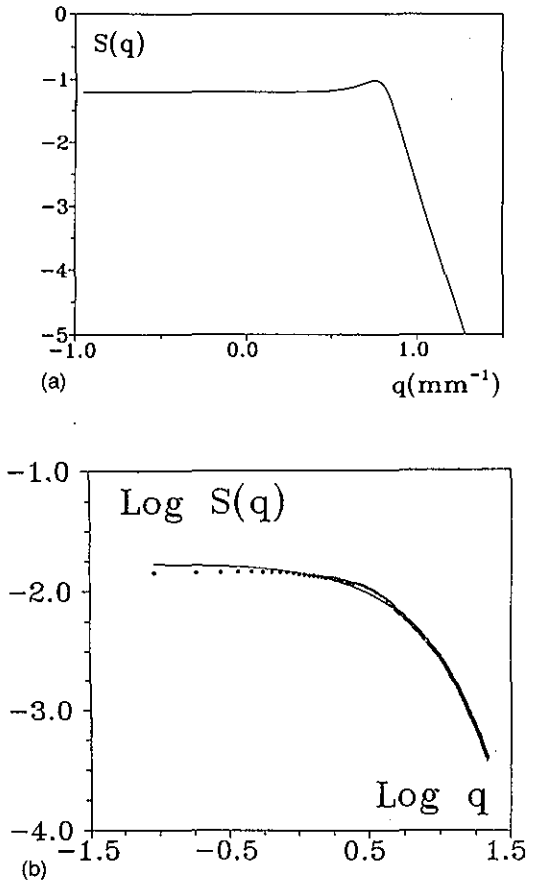

FIG. 5. (a) Wave number time-averaged power spectrum of the optical field for the same experimental parameters as in Fig. 2. Both vertical and horizontal axis are in log scale. (b) Experimental power spectrum from Ref. 20.

mode above threshold feels the global effect of all the modes below threshold as a noise source which washes out the phase relations built by diffraction, thus giving rise to patterns which are independent from boundary conditions (bulk dominated patterns).

The modal equations here introduced have not been solved in their full generality, nor have we attempted a multiple scale analysis leading to various classes of amplitude equations.[37] We have instead limited our approach to the linear region in the boundary and bulk dominated regimes (low and high F, respectively). Furthermore, in the case of a small number of competing modes, we have introduced the leading nonlinearities compatible with the dynamical symmetries of the problem, building normal form equations which yield a time-dependent mode–mode competition. This reduced theoretical approach is sufficient to provide a good qualitative agreement with the wealth of experimental information nowadays available on photorefractive oscillators.

ACKNOWLEDGMENT

Work partly supported by EEC—Esprit Basic Research action TONICS (Contract No. 7118).

[1] A. M. Turing, Philos. Trans. R. Soc. London B **237**, 37 (1952).
[2] Y. Kuramoto, Prog. Theor. Phys. **71**, 1182 (1982); in *Chemical Oscillations, Waves and Turbulence*, edited by H. Haken (Springer-Verlag, Berlin, 1984); P. Coullet, T. Frisch, and G. Sonnino, in *Spatio Temporal Organization in Nonequilibrium Systems*, edited by S. C. Mueller and T. Plesser (Projekt Verlag, Dortmund, 1992), pp. 46–58 and references therein.
[3] B. S. Kerner and V. V. Osipov, Sov. Phys. Usp. **33**, 679 (1990); J. J. Perraud, A. De Wit, E. Dulos, P. De kepper, G. Dewel, and P. Borckmans, Phys. Rev. Lett. **71**, 1272 (1993).
[4] L. A. Lugiato and L. Lefever, Phys. Rev. Lett. **58**, 2209 (1987).
[5] G. D'Alessandro and W. J. Firth, Phys. Rev. Lett. **66**, 2597 (1991); G. D'Alessandro and W. J. Firth, Phys. Rev. A **46**, 537 (1992).
[6] J. Y. Courtois and G. Grynberg, Opt. Commun. **87**, 186 (1992).
[7] S. A. Akhmanov, M. A. Vorontsov, and V. Yu. Ivanov, JETP Lett. **47**, 707 (1988).
[8] R. Macdonald and H. J. Eichler, Opt. Commun. **89**, 289 (1992).
[9] M. Tamburrini, M. Bonavita, S. Wabnitz, and E. Santamato, Opt. Lett. **18**, 855 (1993).
[10] E. Pampaloni, S. Rasidori, and F. T. Arecchi, Europhys. Lett. **24**, 647 (1993); E. Pampaloni, P. L. Ramazza, S. Residori, and F. T. Arecchi, Europhys. Lett. **25**, 587 (1994).
[11] C. Green, G. B. Mindlin, E. J. D'Angelo, H. G. Solari, and J. R. Tredicce, Phys. Rev. Lett. **65**, 3124 (1990); E. J. D'Angelo, E. Izaguirre, G. B. Mindlin, G. Huyet, L. Gil, and J. R. Tredicce, Phys. Rev. Lett. **68**, 3702 (1992).
[12] D. Dangoisse, D. Hennequin, C. Lepers, E. Lovergnaux, and P. Glorieux, Phys. Rev. A **46**, 5955 (1992).
[13] M. Brambilla, M. Cattaneo, L. A. Lugiato, R. Pirovano, F. Prati, A. J. Kent, G. L. Oppo, A. B. Coates, C. O. Weiss, C. Green, E. J. D'Angelo, and J. R. Tredicce, Phys. Rev. A **49**, 1427 (1994) and references therein.
[14] For a review of early works, see, e.g., *Photorefractive Materials and their Applications,* edited by P. Gunter and J. P. Huignard (Springer-Verlag, Berlin, 1989).
[15] F. T. Arecchi, G. Giacomelli, P. L. Ramazza, and S. Residori, Phys. Rev. Lett. **65**, 2531 (1990).
[16] F. T. Arecchi, Physica D **51**, 450 (1991).
[17] F. T. Arecchi, G. Giacomelli, P. L. Ramazza, and S. Residori, Phys. Rev. Lett. **67**, 3749 (1991).
[18] P. L. Ramazza, S. Residori, G. Giacomelli, and F. T. Arecchi, Europhys. Lett. **19**, 475 (1992).
[19] F. T. Arecchi, S. Boccaletti, G. B. Mindlin, and C. Perez Garcia, Phys. Rev. Lett. **69**, 3723 (1992).
[20] F. T. Arecchi, S. Boccaletti, P. L. Ramazza, and S. Residori, Phys. Rev. Lett. **70**, 2277 (1993).
[21] G. Indebetouw and S. Liu, Opt. Commun. **91**, 321 (1992).
[22] D. Hennequin, L. Dambly, D. Dangoisse, and P. Glorieux, J. Opt. Soc. Am. B **11**, 676 (1994).
[23] Theory: P. Hadley and M. Beasley, Appl. Phys. Lett. **50**, 621 (1987); experiment: K. Wiesenfeld, C. Bracikowski, G. James, and R. Roy, Phys. Rev. Lett. **65**, 1749 (1990).
[24] K. Ikeda, K. Matsumoto, and K. Otsuka, Prog. Theor. Phys., Suppl., **99**, 295 (1989).
[25] K. Otsuka, Phys. Rev. Lett. **65**, 329 (1990).
[26] K. Kaneko, Physica D **54**, 5 (1991).
[27] I. Tsuda, Neural Networks **5**, 313 (1992).
[28] P. C. Hohenberg and B. I. Shraiman, Physica D **37**, 109 (1989).
[29] N. V. Kukhtarev, V. B. Markov, S. G. Odulov, M. S. Soskin, and V. L. Vinetskii, Ferroelectrics **22**, 949 (1979).
[30] J. Feinberg, D. Helman, A. R. Tanguay, Jr., and R. W. Hellwarth, J. Appl. Phys. **51**, 1279 (1980).
[31] R. Jaura, T. P. Hall, and P. D. Foote, Opt. Eng. **25**, 1068 (1986).
[32] L. Arizmendi, J. M. Cabrera, and F. Agullo'-Lopez, Int. J. Opt. **7**, 149 (1992).
[33] G. D'Alessandro, Phys. Rev. A **46**, 2791 (1992).
[34] J. W. Goodman, *Introduction to Fourier Optics* (McGraw-Hill, San Francisco, 1968).
[35] M. Golubitsky, I. Stewart, and D. Schaeffer, *Singularities and Groups in Bifurcation Theory*, Applied Mathematical Sciences (Springer-Verlag, New York, 1983), Vol. 69.
[36] G. Dangelmayr and E. Knobloch, Nonlinearity **4**, 399 (1991).
[37] A. C. Newell and J. V. Moloney, *Nonlinear Optics* (Addison–Wesley, Redwood City, CA, 1992).